ISSN 0030-400X, Optics and Spectroscopy, 2014, Vol. 117, No. 1, pp. 152–157. © Pleiades Publishing, Ltd., 2014.
Original Russian Text © V.A. Ushenko, M.I. Sidor, Yu.F. Marchuk, N.V. Pashkovskaya, D.R. Andreichuk, 2014, published in Optika i Spektroskopiya, 2014, Vol. 117, No. 1, pp. 159–165.

PHYSICAL AND GEOMETRICAL OPTICS

Azimuth-Invariant Mueller-Matrix Differentiation of the Optical Anisotropy of Biological Tissues

V. A. Ushenko[a], M. I. Sidor[b], Yu. F. Marchuk[c], N. V. Pashkovskaya[c], and D. R. Andreichuk[c]

[a] *Chernovtsy National University, Chernovtsy, 58012 Ukraine*

[b] *Department of Optics and Spectroscopy, Chernovtsy National University, Chernovtsy, 58012 Ukraine*

[c] *Bukovina State Medical University, Chernovtsy, 58000 Ukraine*

e-mail: yuriyu@gmail.ru

Received November 11, 2013; in final form, December 27, 2013

Abstract—A Mueller-matrix model is proposed for analysis of the optical anisotropy of protein networks of optically thin nondepolarizing layers of biological tissues with allowance for birefringence and dichroism. The model is used to construct algorithms for reconstruction of coordinate distributions of phase shifts and coefficient of linear dichroism. Objective criteria for differentiation of benign and malignant tissues of female genitals are formulated in the framework of the statistical analysis of such distributions. Approaches of evidence-based medicine are used to determine the working characteristics (sensitivity, specificity, and accuracy) of the Mueller-matrix method for the reconstruction of the parameters of optical anisotropy and show its efficiency in the differentiation of benign and malignant tumors.

DOI: 10.1134/S0030400X14070248

INTRODUCTION

Biological tissues are structurally inhomogeneous optically anisotropic absorbing media. The most general approximations using the Mueller-matrix formalism are needed for the analysis of the interaction of polarized radiation with such complicated systems. Various practical methods based on the measurement and analysis of the Mueller matrices of the samples under study are employed in biological and medical study [1–12]. An independent branch of matrix optics that involves the laser polarimetry of histological sections has been developed over the last 10–15 years [13]. The corresponding results were used to establish relationships of the sets of the first- to fourth-order statistical moments [14–19] that characterize the distribution of the Mueller-matrix elements and the parameters of linear birefringence of fibrillar protein networks in human tissues. Such an approach allows the diagnostics of oncological modifications of derma and epithelial and connective tissues of female genitals [20–23]. Note that the effects of the optical anisotropy of biological tissues are not restricted to the linear birefringence. The diagnostic methods can be developed with the aid of circular birefringence and linear and circular dichroism. Note also that most elements of the Mueller matrix are azimuth-dependent. This circumstance leads to a decrease in the accuracy of the clinical polarimetric diagnostics based on the comparative study of relatively large groups of samples.

In this work, we generalize the model of the optical anisotropy of the protein networks and develop a method for the azimuth-stable Mueller-matrix mapping of histological sections for differentiation of inflammatory states of biological tissues.

BRIEF THEORY

The analysis of the optical anisotropy of biological tissues is based on the following model concepts.

(i) Optically thin layers of biological tissues with the absorption coefficient $\tau < 0.1$ serve as objects under study. The polarization modulation of electromagnetic radiation dominates in such samples. In this regard, the samples do not depolarize or transform the polarization of the probe beam. In addition, such layers are classical objects for the widely spread histological analysis.

(ii) Amino acids and polypeptide chains (primary protein structure) exhibit optical activity and can be characterized using the matrix operator [10]

$$\{\Omega\} = \begin{Vmatrix} 1 & 0 & 0 & 0 \\ 0 & \omega_{22} & \omega_{23} & 0 \\ 0 & \omega_{32} & \omega_{33} & 0 \\ 0 & 0 & 0 & 1 \end{Vmatrix}, \quad \begin{matrix} \omega_{22} = \omega_{33} = \cos 2\theta, \\ \omega_{23} = -\omega_{32} = \sin 2\theta. \end{matrix} \qquad (1)$$

Here, θ is the polarization rotation angle for an optical beam that is incident on a protein chain.

(iii) Fibrillar protein networks (secondary structures) that are formed by polypeptide chains exhibit linear birefringence and linear dichroism. The optical

manifestations of such effects are described using the Mueller matrices [10]

$$\{D\} = \begin{Vmatrix} 1 & 0 & 0 & 0 \\ 0 & d_{22} & d_{23} & d_{24} \\ 0 & d_{32} & d_{33} & d_{34} \\ 0 & d_{42} & d_{43} & d_{44} \end{Vmatrix},$$

$$\begin{aligned} d_{22} &= \cos^2 2\rho + \sin^2 2\rho \cos\delta, \\ d_{23} &= -d_{32} = \cos 2\rho \sin 2\rho (1 - \cos\delta), \\ d_{33} &= \sin^2 2\rho + \cos^2 2\rho \cos\delta, \\ d_{24} &= -d_{42} = \sin 2\rho \sin\delta, \\ d_{34} &= -d_{43} = \cos 2\rho \sin\delta, \\ d_{44} &= \cos\delta. \end{aligned} \quad (2)$$

Here, $\{D\}$ is the matrix of linear birefringence in which ρ is the fibril direction and δ is the phase shift between linearly polarized orthogonal components of the optical amplitude. We also have

$$\{\Psi\} = \begin{Vmatrix} 1 & \varphi_{12} & \varphi_{13} & 0 \\ \varphi_{21} & \varphi_{22} & \varphi_{23} & 0 \\ \varphi_{31} & \varphi_{32} & \varphi_{33} & 0 \\ 0 & 0 & 0 & \varphi_{44} \end{Vmatrix},$$

$$\begin{aligned} \varphi_{12} &= \varphi_{21} = (1 - \Delta\tau)\cos 2\rho, \\ \varphi_{13} &= \varphi_{31} = (1 - \Delta\tau)\sin 2\rho, \\ \varphi_{22} &= (1 + \Delta\tau)\cos^2 2\rho + 2\sqrt{\Delta\tau}\sin^2 2\rho, \\ \varphi_{23} &= \varphi_{32} = (1 - \Delta\tau)\sin 2\rho, \\ \varphi_{33} &= (1 + \Delta\tau)\sin^2 2\rho + 2\sqrt{\Delta\tau}\cos^2 2\rho, \\ \varphi_{44} &= 2\sqrt{\Delta\tau}. \end{aligned} \quad (3)$$

Here, $\{\Psi\}$ is the matrix of linear dichroism in which $\Delta\tau = \tau_x/\tau_y$, $\tau_x = \tau\cos\rho$, and $\tau_y = \tau\sin\rho$ (τ_x and τ_y are absorption coefficients for the linearly polarized orthogonal components of the optical amplitude).

(iv) Complicated helical polypeptide protein structures or combinations of such structures (tertiary structure) exhibit circular dichroism. Optical effects related to such structural features can be characterized using the Mueller matrix [10]

$$\{\Phi\} = \begin{Vmatrix} 1 & 0 & 0 & \varphi_{14} \\ 0 & \varphi_{22} & 0 & 0 \\ 0 & 0 & \varphi_{33} & 0 \\ \varphi_{41} & 0 & 0 & 1 \end{Vmatrix},$$

$$\begin{aligned} \varphi_{22} &= \varphi_{33} = (1 - C^2)/(1 + C^2), \\ \varphi_{14} &= \varphi_{41} = \pm 2C/(1 + C^2). \end{aligned} \quad (4)$$

Here, $C = (g_\otimes - g_\oplus)/(g_\otimes + g_\oplus)$ and $g_\otimes$ and $g_\oplus$ are absorption coefficients for the left-hand ($\otimes$) and right-hand ($\oplus$) circularly polarized components of the optical amplitude.

For the above effects of optical anisotropy (expressions (1)–(4)), the Mueller matrix of a layer of biological tissue can be represented as

$$\{M\} = \{\Omega\}\{D\}\{\Psi\}\{\Phi\} = \begin{Vmatrix} 1 & M_{12} & M_{13} & M_{14} \\ M_{21} & M_{22} & M_{23} & M_{24} \\ M_{31} & M_{32} & M_{33} & M_{34} \\ M_{41} & M_{42} & M_{43} & M_{44} \end{Vmatrix}. \quad (5)$$

In the visible spectral range, protein molecules exhibit insignificant absorption. Therefore, matrix (5) is predominantly determined by linear and circular birefringence:

$$\begin{aligned} \{M\} &= \{\Omega\}\{D\} \\ &= \begin{Vmatrix} 1 & 0 & 0 & 0 \\ 0 & (d_{22}\omega_{22} + d_{23}\omega_{32}) & (d_{22}\omega_{23} + d_{23}\omega_{33}) & d_{24} \\ 0 & (d_{32}\omega_{22} + d_{33}\omega_{32}) & (d_{32}\omega_{23} + d_{33}\omega_{33}) & d_{34} \\ 0 & (d_{42}\omega_{22} + d_{43}\omega_{32}) & (d_{42}\omega_{23} + d_{43}\omega_{33}) & d_{44} \end{Vmatrix} \\ &\equiv \begin{Vmatrix} 1 & 0 & 0 & 0 \\ 0 & M_{22} & M_{23} & M_{24} \\ 0 & M_{32} & M_{33} & M_{34} \\ 0 & M_{42} & M_{43} & M_{44} \end{Vmatrix}. \end{aligned} \quad (6)$$

However, only a few elements of Mueller matrix (6) are convenient for analysis of biological samples. In general, eight of the ten nonzero elements are varied when the sample is rotated around the axis of the probe beam. On the other hand, the results of [1, 2, 4] show that the following elements of matrix $\{M\}$ or combinations of such elements are azimuth-stable (i.e., independent of sample rotation angle Θ):

$$\begin{aligned} M_{11}(\Theta) &= \text{const}, \\ M_{44}(\Theta) &= \text{const}, \\ [M_{22} + M_{33}](\Theta) &\equiv \Sigma M_{22;33}(\Theta) = \text{const}, \\ [M_{23} - M_{32}](\Theta) &\equiv \Delta M_{23;32}(\Theta) = \text{const}. \end{aligned} \quad (7)$$

From the physical point of view, the parameters can be used to obtain different characteristics.

Parameter M_{11} characterizes the transformation of laser intensity and represents a normalized parameter of reduced matrix (6).

Parameter $M_{44} \equiv d_{44} = \cos\delta$ characterizes the phase modulation of the optical radiation that passes through birefringent fibrillar networks (see expressions (2) and (6)).

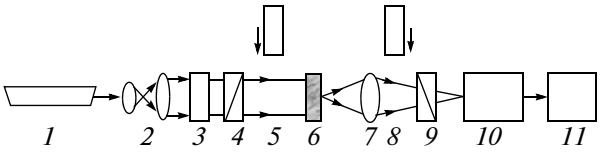

Fig. 1. Optical scheme of polarimeter: (*1*) He–Ne laser, (*2*) collimator, (*3*) stationary quarter-wave plate, (*4*) polarizer, (*5*) and (*8*) movable quarter-wave plates, (*6*) object under study, (*7*) microobjective, (*9*) analyzer, (*10*) CCD camera, and (*11*) PC.

Parameter $\Sigma M_{22;33} = (1 + \cos\delta)\cos 2\theta$ characterizes the mixed modulation of the optical radiation by birefringent fibrils and optically active polypeptide side chains.

Parameter $\Delta M_{23;32} = (1 + \cos\delta)\sin 2\theta$ is also simultaneously determined by the parameters of birefringence and optical activity of the fibrillar network.

Thus, we study two types of azimuth-invariant coordinate distributions:

$$q \equiv \begin{cases} M_{44}(m \times n) \sim \cos\delta, \\ (\Delta M_{23;32}/\Sigma M_{22;33}) \sim \tan 2\theta. \end{cases}$$

OBJECTS, METHODS, AND ALGORITHMS FOR DATA PROCESSING

Optically thin histological sections of excised biological tissues with a geometrical thickness of $d \approx 30$ μm serve as the samples. We study two types of inflammations: calculous cholecystitis (group 1 consisting of 28 samples) and gangrenous cholecystitis (group 2 consisting of 29 samples).

The coordinate distributions of the Muller-matrix elements are measured using a conventional Stokes polarimeter (Fig. 1) [13]. A parallel low-intensity beam of a He–Ne laser with a diameter of $\varnothing = 2 \times 10^3$ μm, a power of $W = 5.0$ mW, and a wavelength of $\lambda = 0.6328$ μm is incident on sample *6*. The incident beam passes through quarter-wave retardation plates *3* and *5* and polarizer *4*. Histological section *6* is sequentially probed using laser beams with linear polarizations at azimuth angles of 0°, 90°, and +45° and right-hand circular polarization (⊗). The images are projected by a Nikon CFI Achromat P polarization microobjective *7* with a focal length of 30 mm, a numerical aperture of 0.1, and a magnification of 4× to the photosensitive plane of a Sony ICX205AL (progressive scan) CCD camera *10* with a size of $m \times n = 800 \times 600$ pixels. The resolution is 1280 × 960, the photosensitive area is 7600×6200 μm^2, the sensitivity is 0.05 1×, the dynamic range is 8 bit, the SNR is 9 bit, and the nonlinearity of the photosensitivity is no greater than 15%. The images of histological sections *6* are analyzed using polarizer *9* and quarter-wave plate *8*. For a series of linearly (0°, 45°, and 90°) and right-hand circularly (⊗) polarized laser beams, we measure parameters of Stokes vector $S_i^{0;45;90;\otimes}$ at $m \times n$ points of digital image:

$$\begin{aligned} S_{i=2}^{0;45;90;\otimes} &= I_0^{0;45;90;\otimes} - I_{90}^{0;45;90;\otimes}, \\ S_{i=3}^{0;45;90;\otimes} &= I_{45}^{0;45;90;\otimes} - I_{135}^{0;45;90;\otimes}, \\ S_{i=4}^{0;45;90;\otimes} &= I_{\otimes}^{0;45;90;\otimes} - I_{\oplus}^{0;45;90;\otimes}. \end{aligned} \quad (8)$$

Here, $I_{0;90;45;135;\otimes;\oplus}^{0;45;90;\otimes}$ are intensities of linearly (0°, 45°, 90°, and 135°) and right-hand (⊗) and left-hand (⊕) circularly polarized components of the laser radiation that are selected using polarizer *9* and quarter-wave plate *8*.

Then, we calculate informative parameters (7) using the following algorithm:

$$M_{11}^{-1} \times \begin{cases} M_{11}, \\ M_{44} = S_4^{\otimes} - 0.5(S_4^0 + S_4^{90}), \\ \Sigma M_{22;33} = M_{22} + M_{33} \\ = 0.5(S_2^0 - S_2^{90}) + S_3^{45} - 0.5(S_3^0 + S_3^{90}), \\ \Delta M_{23;32} = M_{23} - M_{32} \\ = S_2^{45} - 0.5(S_2^0 + S_2^{90}) - 0.5(S_3^0 - S_3^{90}). \end{cases} \quad (9)$$

For the objective estimation of the distributions, we employ statistical analysis and calculate sets of statistical moments (from the first to fourth order):

$$\begin{aligned} Z_1 &= \frac{1}{N}\sum_{j=1}^{N}|q|_j, \quad Z_2 = \sqrt{\frac{1}{N}\sum_{j=1}^{N}(q - Z_1)_j^2}, \\ Z_3 &= \frac{1}{Z_2^3}\frac{1}{N}\sum_{j=1}^{N}(q)_j^3, \quad Z_4 = \frac{1}{Z_2^4}\frac{1}{N}\sum_{j=1}^{N}(q)_j^4. \end{aligned} \quad (10)$$

Here, N is the number of pixels. The parameters characterize mean (Z_1), variance (Z_2), skewness (Z_4), and kurtosis (Z_4) of distributions $q(m \times n)$.

ANALYSIS AND DISCUSSION OF EXPERIMENTAL DATA

Figures 2 and 3 show the results of the measurements of the Mueller-matrix rotational invariants that characterize the optical anisotropy of the histological sections of appendix for both groups. Comparative analysis of the experimental data yields the individual structures for the distributions of the Mueller-matrix rotational invariants with respect to magnitude (panels (a) and (b)) and topology (panels (c) and (d)).

For the sample of group 1, the most probable (P) values of parameters are $P(M_{44}) \sim 0.45$–0.5 and $P(\Delta M_{23;32}/\Sigma M_{22;33}) \sim 0.3$–$0.35$. For the sample of group 2, the most probable (P) values of parameters are $P(M_{44}) \sim 0.8$–0.85 and $P(\Delta M_{23;32}/\Sigma M_{22;33}) \sim 0.1$–$0.15$. The results can be physically interpreted

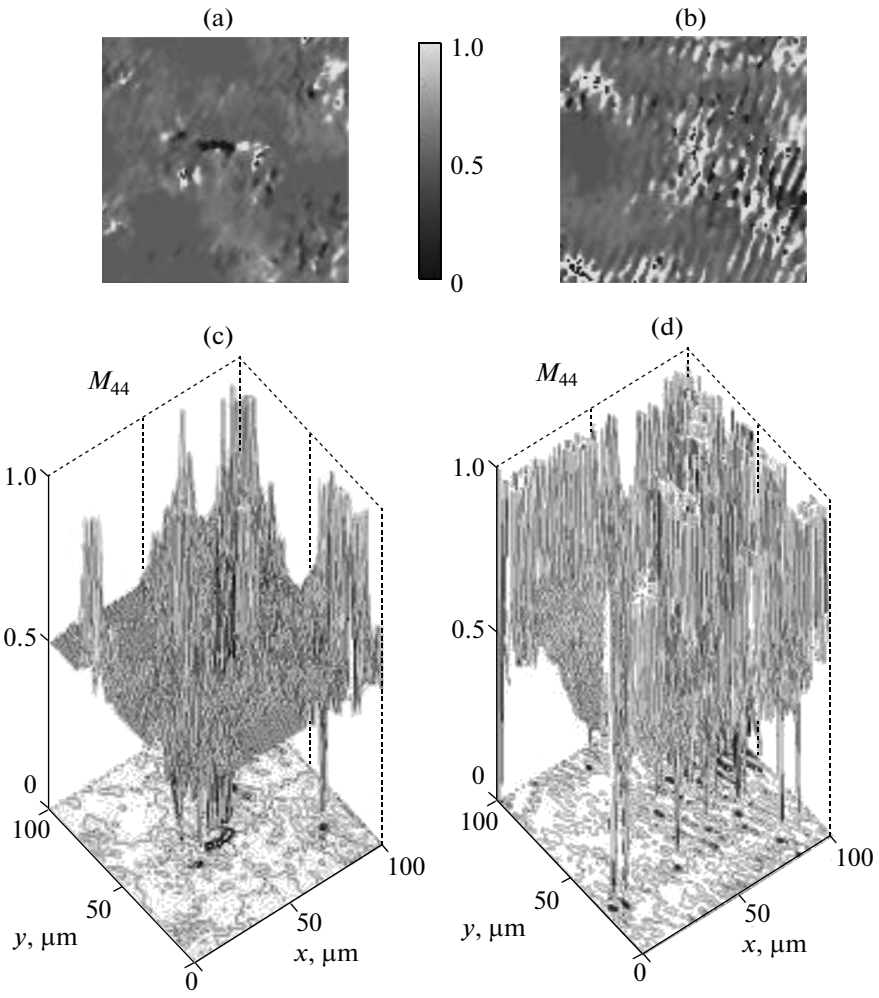

Fig. 2. (a) and (b) 2D and (c) and (d) 3D distributions of matrix element M_{44} for histological sections of (a) and (c) calculous and (b) and (d) gangrenous appendicitis.

using the destruction of the optical anisotropy in the histological sections of the second group (gangrenous appendicitis) owing to the morphological destruction of fibrillar networks. Such a process is most clearly manifested for optically active protein molecules that form fibrillar networks. In an analytical representation, such a scenario corresponds to the following tendencies for the parameters of optical anisotropy: $\delta \to 0$ and $\theta \to 0$. The process can be quantitatively detected with the aid of the corresponding probability variations in the Mueller-matrix invariants:

$$M_{44}(m \times n) \to 1, \quad \Sigma M_{22;33}(m \times n) \to 1, \quad \Delta M_{23;32}(m \times n) \to 0. \tag{11}$$

In the boundary case, the symmetry of the Mueller matrix of the histological section from the second group is transformed into a unit diagonal matrix of the optically isotropic layer:

$$\{M\} \to \begin{Vmatrix} 1 & 0 & 0 & 0 \\ 0 & 1 & 0 & 0 \\ 0 & 0 & 1 & 0 \\ 0 & 0 & 0 & 1 \end{Vmatrix}.$$

For possible clinical application of the Mueller-matrix mapping of the rotational invariants, we perform tests for two statistically reliable groups with confidence interval $p < 0.001$ for samples of both groups. For each group, we determine mean values and standard deviations of statistical moments $Z_{i=1;2;3;4}(q)$ (Table 1) and working characteristics that are normally used in evidence-based medicine: sensitivity $\left(Se = \frac{a}{a+b}100\%\right)$, specificity $\left(Sp = \frac{c}{c+d}100\%\right)$, and accuracy $\left(Ac = \frac{Se+Sp}{2}\right)$, where a and b (c and d) are numbers of correct and incorrect diagnoses, respectively, in group 1 (2) (see Table 2).

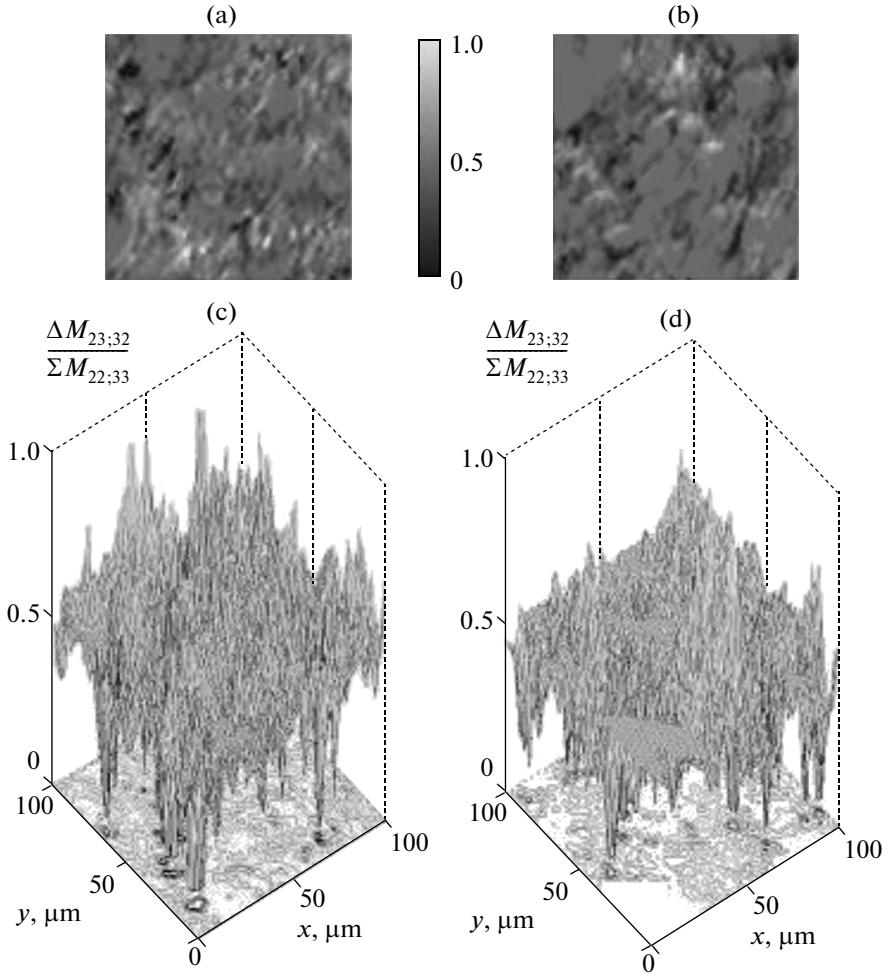

Fig. 3. (a) and (b) 2D and (c) and (d) 3D distributions of Mueller-matrix rotational invariant $\Delta M_{23;32}/\Sigma M_{22;33}$ for histological sections of (a) and (c) calculous and (b) and (d) gangrenous appendicitis.

The most sensitive parameters are statistical moments $Z_{i=1;2;3;4}(q)$ that characterize distributions M_{44} and $\Delta M_{23;32}/\Sigma M_{22;33}$. The following ranges of the group differences are obtained:

$$M_{44}: \quad \Delta Z_1 \leftrightarrow 183, \quad \Delta Z_2 \leftrightarrow 2.88,$$
$$\Delta Z_3 \leftrightarrow 2.19, \quad \Delta Z_4 \leftrightarrow 2.52,$$

$$\Delta M_{23;32}/\Sigma M_{22;33}: \quad \Delta Z_1 \leftrightarrow 1.72, \quad \Delta Z_2 \leftrightarrow 1.55,$$
$$\Delta Z_3 \leftrightarrow 2.04, \quad \Delta Z_4 \leftrightarrow 2.02.$$

The statistical results can be interpreted using the physical analysis of the destruction of the optical anisotropy in the tissue of gangrenous appendix. A decrease in phase shifts ($\delta\downarrow$) is accompanied by an increase in the magnitude and range of variation in matrix element ($(M_{44} = \cos\delta)\uparrow$). Therefore, the mean ($Z_1\uparrow$) and variance ($Z_2\uparrow$) increase and skewness ($Z_3\downarrow$) and kurtosis ($Z_4\downarrow$) decrease for the distribution of this parameter (expression (10)).

A different scenario corresponds to statistical parameters Z_i that characterize the probability distribution of the Mueller-matrix invariant $\Delta M_{23;32}/\Sigma M_{22;33} \sim \tan 2\theta$. The degradation of optical activity ($\theta\downarrow$) is manifested as asymmetric ($Z_3\uparrow$) sharp-peak ($Z_4\uparrow$) distributions of relatively small ($Z_1\downarrow$ and $Z_2\downarrow$) quantities $\Delta M_{23;32}/\Sigma M_{22;33}$ in the plane of the histological section of gangrenous appendix.

Thus, the Mueller-matrix mapping of the rotational invariants of the optical anisotropy of biological tissues is efficient for differential diagnostics of inflammatory processes in appendix: $Ac = 78–83$ and 75–79% for M_{44} ($Ac = 78–83\%$) and $\Delta M_{23;32}/\Sigma M_{22;33}$ ($Ac = 75–79\%$), respectively.

CONCLUSIONS

A method for azimuth-invariant Mueller-matrix mapping has been developed using a model of the gen-

Table 1. First- to fourth-order statistical moments of the distributions of the Mueller-matrix invariants for the histological sections of the calculous and gangrenous appendicitis

Z_i	M_{44}		$\frac{\Delta M_{23;32}}{\Sigma M_{22;33}}$	
	group 1	group 2	group 1	group 2
Z_1	0.47 ± 0.068	0.86 ± 0.11	0.19 ± 0.024	0.11 ± 0.016
Z_2	0.09 ± 0.012	0.26 ± 0.038	0.17 ± 0.019	0.11 ± 0.013
Z_3	1.23 ± 0.18	0.56 ± 0.071	0.83 ± 0.12	1.69 ± 0.19
Z_4	2.19 ± 0.27	0.87 ± 0.12	1.07 ± 0.16	2.15 ± 0.27

Table 2. Working characteristics of the methods for Mueller-matrix mapping

Z_i	M_{44}			$\frac{\Delta M_{23;32}}{\Sigma M_{22;33}}$		
	Se, %	*Sp*, %	*Ac*, %	*Se*, %	*Sp*, %	*Ac*, %
Z_1	84	72	78	78	72	75
Z_2	94	68	81	84	74	79
Z_3	90	76	83	82	74	78
Z_4	92	74	83	84	72	78

eralized optical anisotropy of optically thin layers of biological tissues.

The Mueller-matrix invariants that characterize the polarization effects of optical anisotropy (linear and circular birefringence) have been determined.

In the framework of the statistical approach, we have established a relationship of the first- to fourth-order moments that characterize the Mueller-matrix invariants and variations in the optical anisotropy of appendix tissues.

The diagnostic efficiency of the method for the azimuth-invariant Mueller-matrix mapping has been demonstrated for the differentiation of acute and gangrenous appendicitis.

REFERENCES

1. M. H. Smith, P. Burke, A. Lompado, E. Tanner, and L. W. Hillman, Proc. SPIE—Int. Soc. Opt. Eng. **3991**, 210 (2000).
2. M. H. Smith, Proc. SPIE—Int. Soc. Opt. Eng. **4257**, 82 (2001).
3. Yu. A. Ushenko, Ukr. J. Phys. Opt. **6**, 63 (2005).
4. T. T. Tower, Biophys. J. **81**, 2954 (2001).
5. J. M. Bueno and J. Jaronski, Ophthalmol. Physiol. Opt. **21**, 384 (2001).
6. J. M. Bueno and F. Vargas-Martin, Appl. Opt. **41**, 116 (2002).
7. J. M. Bueno and M. C. W. Campbell, Ophthalmol. Physiol. Opt. **23**, 109 (2003).
8. T. T. Tower and R. T. Tranquillo, Biophys. J. **81**, 2964 (2001).
9. M. Shribak and R. Oldenbourg, Appl. Opt. **42**, 3009 (2003).
10. O. V. Angelsky, A. G. Ushenko, D. N. Burkovets, and Y. A. Ushenko, J. Biomed. Opt. **10**, 014010 (2005).
11. A. Y. Bekshaev, O. V. Angelsky, S. G. Hanson, and C. Y. Zenkova, Phys. Rev. A **86**, 023847 (2012).
12. O. V. Angelsky, P. V. Polyanskii, and C. V. Felde, Opt. Photonics News **23**, 25 (2012).
13. Y. A. Ushenko, J. Biomed. Opt. **16**, 066006 (2011).
14. O. V. Angelsky, S. G. Hanson, A. P. Maksimyak, and P. P. Maksimyak, Opt. Express **13**, 4396 (2005).
15. Yu. A. Ushenko, Yu. Yu. Tomka, and A. V. Dubolazov, Opt. Spektrosk.**110** (6), 814 (2011).
16. O. V. Angelsky, A. G. Ushenko, D. N. Burkovets, and Yu. A. Ushenko, Opt. Appl. **32**, 591 (2002).
17. Y. A. Ushenko, I. Z. Misevich, O. Y. Telenga, Y. Y. Tomka, and A. O. Karachevtsev, Optical Memory and Neural Networks (Information Optics) **20**, 59 (2011).
18. Y. O. Ushenko, Y. Y. Tomka, I. Z. Misevitch, V. V. Istratyy, and O. I. Telenga, Opt. Eng. **50**, 039001 (2011).
19. O. V. Angelsky, A. G. Ushenko, D. N. Burkovets, Yu. A. Ushenko, R. Jozwicki, and K. Patorski, Opt. Appl. **32**, 603 (2002).
20. Yu. A. Ushenko, Yu. Ya. Tomka, A. V. Dubolazov, and O. Yu. Telen'ga, Quantum Electron. **41**, 273 (2011).
21. Y. A. Ushenko, Opto-electron. Rev. **19**, 425 (2011).
22. Y. A. Ushenko, Opto-electron. Rev. **19**, 333 (2011).
23. Yu. A. Ushenko, J. Innov. Opt. Health Sci. **5**, 1150001 (2012).

Translated by A. Chikishev